The effect of isotopic substitution on the excitation of CCS isotopologues in molecular clouds

A Godard Palluet, François Lique

MNRAS **000**, 1–10 (2023) Preprint 13 November 2023 Compiled using MNRAS LATEX style file v3.0

The effect of isotopic substitution on the excitation of CCS isotopologues in molecular clouds

Amélie Godard Palluet[1]★ François Lique,[1]†
[1]*Université de Rennes, CNRS, IPR (Institut de Physique de Rennes) - UMR 6251, F-35000 Rennes, France*

Last updated 2020 June 10; in original form 2013 September 5

ABSTRACT

CCS($^3\Sigma^-$) is one of the few molecules which presents many observable isotopologues, with the reported detection of ^{13}CCS, C^{13}CS, CC^{34}S, and CC^{33}S. The accurate determination of CCS isotopologues abundances allow the study of the isotopic fraction in media where they are detected, and give insights on their formation pathways. The availability of collisional rate coefficients, that are prerequisite for accurate determination of their abundances in astrophysical media under non-local thermodynamic equilibrium (LTE) conditions, allows drawing reliable conclusions on their abundances. In this study, fine and hyperfine-structure resolved rate coefficients induced by collisions with helium are produced with a quantum approach for all detected CCS isotopologues for the 5-50 K temperature range. Radiative transfer models have been performed with the new data to discuss their impact on the excitation conditions of these species. The isotopic substitution effect appears to be weak between fine-structure rate coefficients. The observed lines of CCS, ^{13}CCS, C^{13}CS and CC^{34}S are found to be out of LTE conditions, and therefore, the proper determination of the abundance of CCS isotopologues in molecular clouds requires the use of the data produced in this work.

Key words: Scattering – Molecular data – Radiative transfer – Molecular processes

1 INTRODUCTION

The CCS ($^3\Sigma^-$) radical was detected in many astronomical sources, especially in molecular clouds where it is known to be a good tracer of physical conditions and evolution stages (Suzuki et al. 1992; Velusamy et al. 1995). However, an accurate determination of its abundance in these media, which not statisfy local thermodynamic equilibrium (LTE) conditions, requires the use of inelastic rate coefficients.

Due to the presence of an electronic spin and a large spin-splitting, CCS very peculiar internal structure is difficult to take into account in rate coefficients calculations. Up to now, the analysis of CCS observations has been done, either under LTE assumption, either with approximated rate coefficients derived from OCS-H_2 rotational rate coefficients (Fuente et al. 1990; Suzuki et al. 1992), or obtained from OCS-H_2 potential energy surface (PES) (Wolkovitch et al. 1997). To overcome this lack of data, Godard Palluet & Lique (2023) (hereafter Paper I) performed full quantum scattering calculations based on the first CCS-He PES computed from highly correlated methods. In this work, He is used as a template for H_2, the dominant collisional partner in molecular clouds and circumstellar enveloppe. The use of He as a substitute for H_2 could lead to significant uncertainties in case of collisions with light hydrides but is expected to be reasonably accurate for heavy molecules (Wernli et al. 2007) such as CCS. In Paper I, the authors derived the first accurate set of CCS-He fine-structure resolved rate coefficients for the 5-50 K temperature range. These new rate coefficients have been shown to be in strong disagreement with previous data suggesting significant inaccuracies on former non-LTE models of CCS.

Four secondary isotopologues of CCS have been currently detected in molecular clouds: ^{13}CCS; C^{13}CS; CC^{34}S (Ikeda et al. 1997) and CC^{33}S (Fuentetaja et al. 2023). It is one of the few molecules to present many observable isotopologues.

The isotopic fraction ^{12}C/^{13}C, ^{32}S/^{33}S and ^{32}S/^{34}S is one of the best tool to follow the chemical evolution of molecular clouds and planetary systems bodies (Hily-Blant et al. 2018; Loison et al. 2020). The abundance ratio between ^{13}C-bearing isotopologues can also be used to constraint the production path of interstellar molecules, as done for HC_3N and HC_5N by Takano et al. (1998); Taniguchi et al. (2016), and also for CCH and CCS by Sakai et al. (2007). The later study found an abundance ratio [C^{13}CS]/[^{13}CCS] of 4.2 in TMC-1, which cannot be explained by zero-point energy differences. However, it was derived based on LTE assumptions so it might be over(under)estimated.

No rate coefficients have been reported for any of the isotopologues of CCS. Indeed, in addition to the complex fine structure of CCS radicals, ^{13}C ($I = \frac{1}{2}$) and ^{33}S ($I = \frac{3}{2}$) present a nuclear spin from

★ E-mail: amelie.godard@univ-rennes.fr
† E-mail: francois.lique@univ-rennes.fr

which hyperfine structures arise, making the rate coefficients even more complicated to compute. Therefore, the abundance of CCS secondary isotopologues have always been derived assuming LTE conditions. It is know however that this assumption does not hold in molecular clouds where these isotopologues have been detected.

Previous works of Faure & Lique (2012); Dumouchel et al. (2012); Flower & Lique (2015); Navarro-Almaida et al. (2023) demonstrated the need of isotopologue rate coefficients.

The isotopic substitution of one ^{12}C by one ^{13}C in rate coefficients calculations have been studied for CN (Flower & Lique 2015), CO (Dagdigian 2022), CCH (Pirlot Jankowiak et al. 2023a), and HCN/HNC (Navarro-Almaida et al. 2023). These studies report an effect of about 20-30% on the magnitude of collisional rate coefficients, with no predictible pattern however. Given that such deviation could have an impact on radiative transfer analysis, it might be important to compute isotopologue-specific rate coefficients and not to derive them from CCS data. To the best of our knowledge, rate coefficients for a molecule where the ^{32}S have been substituted by either ^{33}S or ^{34}S have never been reported.

In this paper, we present the first accurate state-to-state inelastic rate coefficients for ^{13}C^{12}C^{12}S; ^{12}C^{13}C^{32}S; ^{12}C^{12}C^{34}S; ^{12}C^{12}C^{33}S in collision with He and we test the impact of CCS isotopologue-specific rate coefficients on non-LTE models.

The five isotopologues discussed here have a $^3\Sigma^-$ ground electronic state, from which a fine structure arise (Section 2.2.2). ^{13}CCS, C^{13}CS and CC^{33}S isotopologues add an hyperfine structure to this fine structure due to non-zero nuclear spin of ^{13}C ($I = \frac{1}{2}$), and ^{33}S ($I = \frac{3}{2}$) (see Section 2.2.3).

The potential energy surface (PES) provided in Paper I was adapted for each isotopologue to perform scattering calculations with the Close-Coupling (CC) approach. On this basis, fine-structure resolved rate coefficients for the 5-50 K temperature range were provided and the recoupling approach was then applied to obtain hyperfine-structure resolved rate coefficients in the 5-15 K temperature range for ^{13}CCS, C^{13}CS and CC^{33}S isotopologues (see Section 2.1 and 2.2). Fine and hyperfine inelastic rate coefficients as well as the effect of the isotopic substitution on these data are presented in Section 3.1 and 3.2. The impact of the rate coefficients on radiative transfer models are discussed in Section 3.3. Finally, Section 4 presents concluding remarks.

2 METHODS

2.1 Potential energy surfaces

The potential energy surface (PES) used to model the collison between CCS isotopologues and helium is the one computed in Paper I. In the later, the PES have been computed for the ^{12}C^{12}C^{32}S-He collisional system. It was described using Jacobi coordinates with a radial parameter R, the distance between G, the center of mass (noted hereafter c.o.m.) of CCS and the He atom, and an angular parameter θ, the angle between the internuclear axis and R, as represented in Figure 1. CCS internuclear distances were fixed at experimental equilibrium geometry $r_{C-S} = 2.96a_0$ and $r_{C-C} = 2.47a_0$.

The interaction potential was computed assuming CCS as a rigid rotor, using the unrestricted coupled cluster single double and perturbative triple excitation [UCCSD(T)] *ab initio* method (Deegan & Knowles 1994), along with the augmented correlation consistent quadruple-zeta basis set (aug-cc-pVQZ) including additional mid-bond functions as defined by Cybulski & Toczyłowski (1999). The

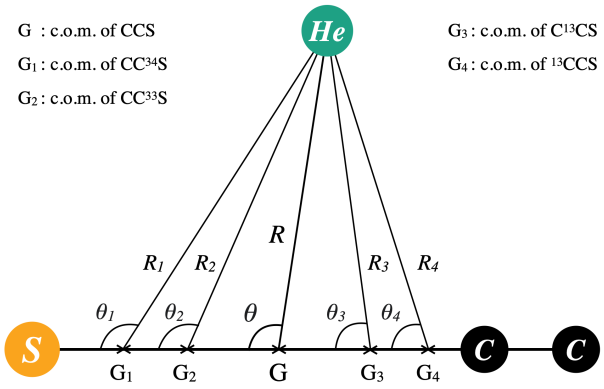

Figure 1. Representation of CCS isotopologues in collision with He in Jacobi coordinates.

basis set superposition error was corrected at each geometry with the counterpoise procedure of Boys & Bernardi (1970). Further details about the PES can be found in Paper I.

Within the Born-Oppenheimer approximation, the PES is valid for all CCS isotopologues which are all linear in their ground electronic state, assuming that the isotopic substitution will not affect the internuclear distances. However, a correction to the position of the c.o.m. must be applied. Indeed, in the Jacobi coordinate system, the origin of the frame is on the c.o.m. of the target molecule, which is not the same for all CCS isotopologues. Thus, the coordinate system of the PES is corrected according to the c.o.m. position, as represented in Figure 1. When the ^{32}S is substituted by ^{34}S or ^{33}S, the c.o.m., G_1 and G_2 respectively, are shifted closer to the sulfur atom according to G. On the contrary, if one of the ^{12}C is substituted by ^{13}C, the c.o.m. is shifted closer to the centered carbon according to G. The proper Jacobi coordinates for the nth CCS isotopologue are then R_n, and θ_n.

As requiered for scattering calculations, the PES for each CCS isotopologues is expressed in terms of Legendre polynomials as:

$$V(R_n, \theta_n) = \sum_{\lambda=0}^{\lambda_{max}} v_\lambda(R_n) P_\lambda(\cos\theta_n) \quad (1)$$

where R_n is the distance between the center of mass G_n of the nth CCS istopologues and the He atom, and θ_n is the angle between the axis of the molecule and R_n, as shown in Figure 1.

2.2 Scattering calculations

2.2.1 *Fine and hyperfine structure of CCS isotopologues*

This study aims at producing accurate state-to-state rate coefficients for CCS isotopologues in collisions with He. Therefore, the proper structure of each CCS isotopologue needs to be taken into account. This is even more true for CCS which presents a large spin-splitting, leading to a peculiar fine structure. Indeed, accurately taking into account the structure of CCS in the scattering calculations have been proven to have a signifcant impact on the rate coefficients in Paper I.

All CCS isotopologues are $^3\Sigma^-$ in their electronic ground state. Therefore, a coupling between the electronic spin S and the rotational angular momentum of the radical N occurs. This so-called spin-rotation coupling will split the rotational levels into fine structure levels.

Table 1. Spectroscopic constants of CCS, ^{13}CCS, C^{13}CS, and CC^{34}S isotopologues from McGuire et al. (2018), and of CC^{33}S from Fuentetaja et al. (2023). The values in brackets are theoretical values.

Spectroscopic constants (cm^{-1})	CCS	^{13}CCS	C^{13}CS	CC^{34}S	CC^{33}S
B	0.216074	0.206412	0.215048	0.211342	0.213630
$D \times 10^8$	5.760985	5.243628	5.710284	5.518151	[5.763988]
$\gamma_0 \times 10^4$	-4.907061	-4.689911	-4.880043	-4.798653	[-4.916]
λ_0	3.242098	3.242376	3.243134	3.242080	3.242934

The total angular momentum j of the molecule is then expressed as:

$$\mathbf{j} = \mathbf{N} + \mathbf{S} \tag{2}$$

The molecular Hamiltonian H included in the scattering calculations is

$$H = H_{rot} + H_{sr} + H_{ss} \tag{3}$$

where H_{rot}, H_{sr} and H_{ss} denote for the rotational, spin-rotation, and spin-spin terms, respectively. They are given by

$$H_{rot} = BN^2 - DN^4$$
$$H_{sr} = \gamma_0 (N \cdot S)$$
$$H_{ss} = \frac{2}{3}\lambda_0 (3S_z - S)$$

where B is the rotational constant of the molecule, D the centrifugal distorsion constant, γ_0 the spin-rotation interaction constant, and λ_0 the spin-spin interaction constant.

The fine-structure energy levels are described with the intermediate coupling representation. The rotational wavefunctions for CCS isotopologues for $j \geq 1$ within the intermediate coupling scheme is written as (Alexander & Dagdigian 1983)

$$\begin{aligned} |F_1 jm\rangle &= \cos\alpha |N = j-1, Sjm\rangle + \sin\alpha |N = j+1, Sjm\rangle, \\ |F_2 jm\rangle &= |N = j, Sjm\rangle, \\ |F_3 jm\rangle &= -\sin\alpha |N = j-1, Sjm\rangle + \cos\alpha |N = j+1, Sjm\rangle, \end{aligned} \tag{4}$$

where α described the mixing angle between pure Hund's case (b) basis functions $|N, Sjm\rangle$. In pure Hund's case (b) limit, $\alpha \rightarrow 0$ and the F_1, F_2, and F_3 fine structure levels will correspond to $N = j$ - 1, $N = j$, and $N = j + 1$, respectively. Hereafter, each fine structure energy level will be labeled as for pure Hund's case (b) by the couple of quantum numbers N_j according to the usual astrophysical notation.

The spectroscopic constants used here, presented in Table 1, were taken from McGuire et al. (2018) for CCS, ^{13}CCS, C^{13}CS, and CC^{34}S isotopologues, and from Fuentetaja et al. (2023) for the CC^{33}S isotopologue.

These constants are quite similar for all isotopologues, leading to very similar fine structure, as one can see in Table A1. What matters is that the order of levels remains consistent between all isotopologues since it could have affected the rate coefficients if the transition is an excitation in some isotopologues and de-excitations in others.

If one of the atom of the molecule presents a non-zero nuclear spin, then a coupling will occur between the nuclear spin I of the atom and the angular momentum j, leading to a splitting of the fine structure energy levels into hyperfine structure energy levels. In that case, the correct quantum number F is now defined as:

$$\mathbf{F} = \mathbf{j} + \mathbf{I} \tag{5}$$

In this study, three of the five isotopologues considered present an hyperfine structure: ^{13}CCS, C^{13}CS, and CC^{33}S. The nuclear spin I of the ^{13}C atom being equal to $\frac{1}{2}$, each fine structure level with $j \geq 1$ will be splitted into two hyperfine levels. The nuclear spin of the ^{33}S atom $I = \frac{3}{2}$, so each fine structure level with $j \geq 2$ energy levels will be splitted into four hyperfine energy levels (and only in three hyperfine structure energy levels for $j = 1$).

2.2.2 *Fine structure resolved rate coefficients*

In astrophysical media, only levels with an internal energy ≤ 100 cm^{-1} can be considered as significantly populated at 50 K. Scattering calculations were performed for all isotopologues to produce converged fine structure excitation cross-sections between levels up to $N_j = 20_j$, which are below the first excited bending mode ν_2 = 134 cm^{-1}. Thus, rate coefficients are obtained for all transitions between the first 61 fine structure levels of the isotopologues.

Calculations for all CCS isotopologues reported in the present paper were carried out by taking into account the exact energy splitting of the levels as well as rotational wavefunction that are linear combination of pure Hund's case (b), as defined in Eq. 4. Inelastic cross sections from an initial state N_j to a final one $N'_{j'}$ are given by the following formula (Alexander & Dagdigian 1983)

$$\sigma_{N_j \rightarrow N'_{j'}} = \frac{\pi}{(2j+1)k^2_{N_j}} \times \sum_{jll'} (2J+1) |\delta_{NN'} \delta_{jj'} \delta_{ll'} - S^J(N_j l; N'_{j'} l')|^2 \tag{6}$$

where l is the angular momentum of the whole complex, $k^2_{N_j} = \frac{2\mu}{\hbar^2}[E - E_{N_j}]$ with E is the total energy of the system, and E_{N_j} is the energy of the N_j level.

The scattering matrices $S^J(N_j l; N'_{j'} l')$ were computed for each total energy E with the Close-Coupling (CC) approach and the log-derivative propagator of Manolopoulos (1986) as implemented in the MOLSCAT code from Hutson & Green (1994). To ensure the convergence of the rate coefficients, cross sections were computed for a total energy from 0.5 cm^{-1} up to 600 cm^{-1} with a various energy step in order to accurately describe their resonances.

Some parameters are constrained by the analytical representation of the PES, as the minimum distance of propagation R_{min} set at 4.36a$_0$ and the number of radial coefficients used to describe the PES λ_{max} set at 31. Other parameters were converged to guarantee that the cross sections are converged to better than 2%. The total angular momentum J_{max} of the system was automatically converged by the MOLSCAT code. More details about the scattering calculations can be found in Paper I since the strategy used for all isotopologues was very similar to that used for the ^{12}C^{12}C^{32}S-He collisional system.

Rate coefficients are then computed from the cross sections assuming a Maxwell-Boltzmann distribution of kinetic energies, as

$$k_{N_j \rightarrow N'_{j'}}(T) = \left(\frac{8k_B T}{\pi\mu}\right)^{1/2} \left(\frac{1}{k_B T}\right)^2 \int_0^\infty E_k \sigma_{N_j \rightarrow N'_{j'}}(E_k) e^{-E_k/k_B T} dE_k, \tag{7}$$

with k_B the Boltzmann constant.

2.2.3 *Hyperfine-structure resolved rate coefficients*

^{13}CCS, C^{13}CS, and CC^{33}S isotopologues have been detected only in molecular clouds, and thus to limit the CPU cost, we decided to

restrict our calculations to the 5-15 K temperature range. Thus the highest hyperfine level taken into account is the 10_{10}, F_i level at ~ 30 cm^{-1}.

In order to take into account the hyperfine structure of the ^{13}CCS, C^{13}CS, and CC^{33}S isotopologues into the rate coefficients calculations, the recoupling method was used. In this approximation, the hyperfine cross sections will be infered from the nuclear spin free S-matrices $S^J(N_j l; N'_{j'} l')$, that were here obtained from the full quantum close-coupling approach. This approximation holds if the splitting between hyperfine energy levels is small compared to the splitting between fine energy levels. In the case of CCS isotopologues, the typical splitting between hyperfine levels is of the order of ~ 10^{-3} cm^{-1}. Consequently, this approach can be considered valid.

The hyperfine cross sections are then obtained based on the S-matrices $S^J(N_j l; N'_{j'} l')$ given by Eq. 6, as defined by Alexander & Dagdigian (1985)

$$\sigma^{REC}_{N_j F \to N'_{j'} F'} = \frac{\pi}{k^2_{N_j F}} (2F'+1) \sum_K \begin{Bmatrix} j & j' & K \\ F' & F & I \end{Bmatrix}^2 P^K(N_j \to N'_{j'}) \tag{8}$$

with

$$P^K(N_j \to N'_{j'}) = \frac{1}{2K+1} \sum_{ll'} |T^K(N_j l; N'_{j'} l')|^2 \tag{9}$$

and

$$T^K(N_j l; N'_{j'} l') = (-1)^{-j-l'} (2K+1) \sum_J (-1)^J (2J+1) \tag{10}$$

$$\times \begin{Bmatrix} l' & j' & J \\ j & l & K \end{Bmatrix} (\delta_{NN'} \delta_{jj'} \delta_{ll'} - S^J(N_j l; N'_{j'} l')) \tag{11}$$

where $|F - F'| \leq K \leq F + F'$.

Once the cross sections are defined, the associated rate coefficients can be infered by averaging these cross sections over the collisional energies, as in Eq. 7.

2.3 Radiative transfer calculations

Rate coefficients are key ingredients to interpret astrophysical observations of molecules through radiative transfer models.

In order to discuss the impact of the rate coefficients produced in this work on the interpretation of observations, non-LTE radiative transfer calculations were performed with the RADEX code (van der Tak et al. 2007) to derive astrophysically relevant quantities, such as excitation temperature T_{ex}, and radiance temperature T_r. It is based on the escape probability formalism. It assumes an isothermal and homogeneous medium, which is fully contained in the antenna beam.

For such modeling, it was assumed that the background radiation field was the cosmic microwave background (CMB) of 2.73 K. The line width was set at 1.0 km.s^{-1}, and the kinetic temperature of the gas at 10 K, the typical temperature of dense molecular clouds (McGuire 2022).

To properly model CCS isotopologues, rate coefficients for CCS in collisions with both He and H_2 are required. A well known approximation to infer rate coefficients with H_2 collider from rate coefficients with He collider is to multiply the datasets by a factor of ~ 1.39, the square-root of the reduced mass ratio.

The Einstein coefficients used were those available in CDMS (Müller et al. 2001, 2005; Endres et al. 2016), and JPL (Pickett et al. 1998) databases.

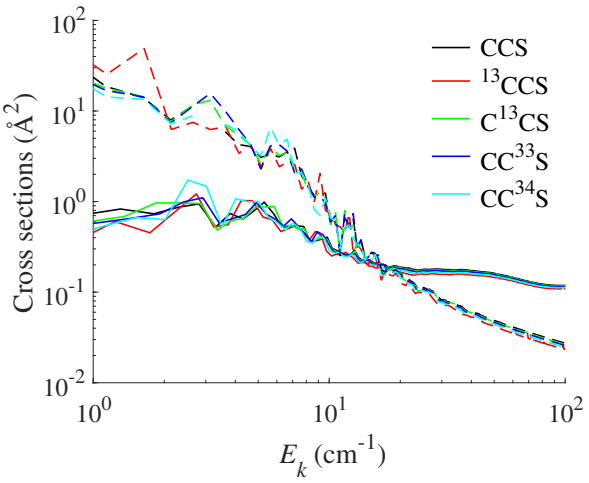

Figure 2. Fine-structure resolved cross sections of CCS, ^{13}CCS, C^{13}CS, CC^{33}S and CC^{34}S for the 6_7-5_4 (solid lines) and the 0_1-1_0 (dashed lines) de-excitation transitions.

3 RESULTS AND DISSCUSSION

3.1 Fine structure resolved cross sections and rate coefficients

Fine structure resolved cross sections were produced according to the methodology described un Section 2.2.2.

Figure 2 shows the collisional energy dependence of the de-excitation fine-structure resolved cross sections for the 6_7-5_4 and the 0_1-1_0 transitions for all 5 CCS isotopologues.

At low kinetic energy, one observe Feshbach and shape resonances that are typical when the collisional energy is lower than the well depth (here about 37 cm^{-1}). They are due to the temporary formation of (quasi)bound states before the complex dissociates (Costes & Naulin 2016).

The behavior and values of the cross sections for all isotopologues are very similar. Some differences can be seen in the resonances area that are by nature very sensitive to the shape of the potential and to the spectroscopic constants. However, the overall isotopic substitution effect is rather small even in the resonance part due to similar spectroscopic constants (see Table 1), and small shift in the c.o.m. positions induced by the isotopic substitution (δ_{G/G_1} = -0.06395a_0 and δ_{G/G_2} = -0.0205a_0, δ_{G/G_3} = 0.03155a_0 ; δ_{G/G_4} = 0.06193a_0). When the resonances disappear (E_k > 37 cm^{-1}), the cross sections are almost identical.

Fine-structure resolved rate coefficients for ^{13}CCS, C^{13}CS, CC^{34}S and CC^{33}S in collision with He have been provided for the 5-50 K temperature range based on the fine-structure resolved cross sections. The fine-structure resolved rate coefficients of ^{12}C^{12}C^{32}S-He have already been provided in Paper I in the same temperature range.

In Paper I, the propensity rules governing CCS-He fine-structure resolved rate coefficients were investigated, with a par-

ticular emphasis on the impact of CCS's peculiar fine structure on these rules. The following propensity rules were determined:

(i) Rate coefficients generally decrease with increasing ΔN, which is the usual behavior for rotational rate coefficients
(ii) Even ΔN transitions are favoured compared to odd ΔN due to larger even anisotropy of the PES caused by its near-homonuclearity
(iii) $\Delta N = \Delta j$ transitions are strongly favoured, as generally observed in molecules in the $^3\Sigma^-$ electronic state

These propensity rules have been found for all CCS isotopologues adressed in this work.

In order to evaluate the influence of the isotopic substitution on CCS isotopologues rate coefficients, a systematic comparison of CCS fine-structure resolved rate coefficients and with those of its secondary isotopologues is presented in Figure 3 and Figure 4 for the isotopic substitution of one of the ^{12}C and of the ^{32}S, respectively. Only de-excitation rate coefficients are taken into account to avoid bias from threshold effects. Only transitions between the first 31 levels are represented for the sake of clarity, but the weighted mean error factor (WMEF) calculated takes into account the de-excitation rate coefficients between all 61 fine-structure levels included in the scattering calculations. The WMEF, defined as in Eq. 12, represents the deviation between the rate coefficients of the main isotopologue and those of the secondary isotopologues, pondered by the highest rate coefficients. This indicator is important to estimate the relevance of the deviation between the two sets of data on non-LTE models, where dominant transitions have more impact.

$$WMEF = \frac{\sum_i k_i^{main} r_i}{\sum_i k_i^{main}} \tag{12}$$

where $r_i = max(k_i^{main}/k_i^{sec}; k_i^{sec}/k_i^{main}) \geq 1$, with k_i^{main} and k_i^{sec} rate coefficients for the i^{th} transition of the main isotopologue ^{12}C^{12}C^{32}S and of the secondary isotopologue considered, respectively.

In Figure 3, rate coefficients of ^{13}C-bearing isotopologues reproduce the rate coefficients of the main isotopologue at better than 10% for C^{13}CS, and at better than 30% for ^{13}CCS at both 10 K (red diamonds) and 50 K (black circles). The discrepancies are larger for the ^{13}CCS isotopologue, which shift to the c.o.m. is larger than for the C^{13}CS isotopologue.

In Figure 4, the overall agreement between the fine-structure resolved rate coefficients induced by the substitution of ^{32}S with either ^{33}S (upper panel) or ^{34}S (lower panel) in the rate coefficients is better than 20% for all transitions at both temperatures considered. The WMEF for both isotopologues is small, but is slightly larger for CC^{34}S than for CC^{33}S. The fact that the data sets are similar is justified by comparable reduced mass, spectroscopic constants, and PES shift. This observation is consistent with previous conclusions drawn for the ^{12}C substitution.

For both ^{12}C and ^{32}S isotopic substitution, the overall effect of isotopic substitution on the fine-structure resolved rate coefficients appears to be weak, with WMEF < 1.05 for all isotopologues. No temperature effect on the WMEF is reported for all isotopologues. Also, the sets of fine rate coefficients for ^{13}CCS and CC^{34}S were also compared (not shown here) since they both exhibit the largest deviations compared to the reference. However, even in that case, the discrepancies exhibited were small, and the WMEF values are of about 1.01 and 1.02 at 10 K and 50 K, respectively. One can concude that the effect of isotopic substititution in CCS molecule is weak and much lower than previously found for non-hydrides molecules (Faure & Lique 2012; Flower & Lique 2015; Navarro-Almaida et al. 2023).

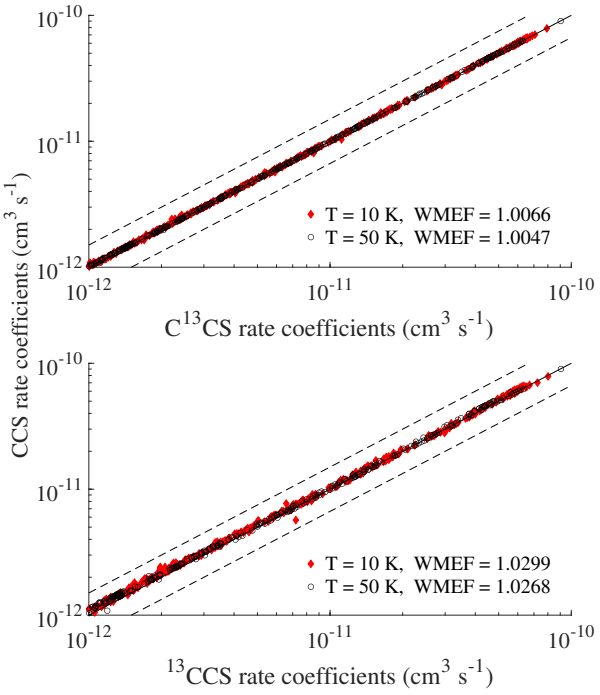

Figure 3. Systematic comparison of de-excitation fine-structure resolved rate coefficients at T = 10 K and 50 K of ^{12}C^{13}C^{32}S (upper panel) and ^{13}C^{12}C^{32}S (lower panel) isotopologues with respect to the fine rate coefficients of the main isotopologue ^{12}C^{12}C^{32}S. The solid line represents a perfect agreement, and the dashed line a deviation of 50%.

3.2 Hyperfine-structure resolved cross sections and rate coefficients

Hyperfine structures of ^{13}CCS, C^{13}CS and CC^{33}S induced by the nuclear spin of ^{13}C ($I = \frac{1}{2}$) and of ^{33}S ($I = \frac{3}{2}$) were taken into account to compute hyperfine-structure resolved cross sections and rate coefficients according to the methodology presented in Section 2.2.3.

The propensity rules of the hyperfine-structure resolved rate coefficients for ^{13}CCS (black) and C^{13}CS (green) are presented at 10 K in Figure 5. The influence of ΔF value is investigated for $\Delta N = \Delta j$ (left panel) and $\Delta N \neq \Delta j$ (right panel) transitions.

Figure 5 exhibits that both ^{13}CCS (black) and C^{13}CS (green) do respect the same the propensity rules, so all following conclusions hold for both these isotopologues.

A clear propensity is in favor of $\Delta F = \Delta j$ transitions for both $\Delta N = \Delta j$ (left panel) and $\Delta N \neq \Delta j$ (right panel) transitions. This is typical of systems with hyperfine structure, due to 6-j Wigner's symbol used in the recoupling technique and has been predicted by Dixon & Field (1979); Alexander & Dagdigian (1985) and confirmed experimentally by Alexander & Dagdigian (1985). It has been already observed in other systems (Daniel et al. 2004; Dumouchel et al. 2012; Kalugina et al. 2012; Buffa 2012; Lique et al. 2016; Dumouchel et al. 2017; Dagdigian 2018; Ndaw et al. 2021; Pirlot Jankowiak et al. 2023a,b). In addition, the dominance of ΔF

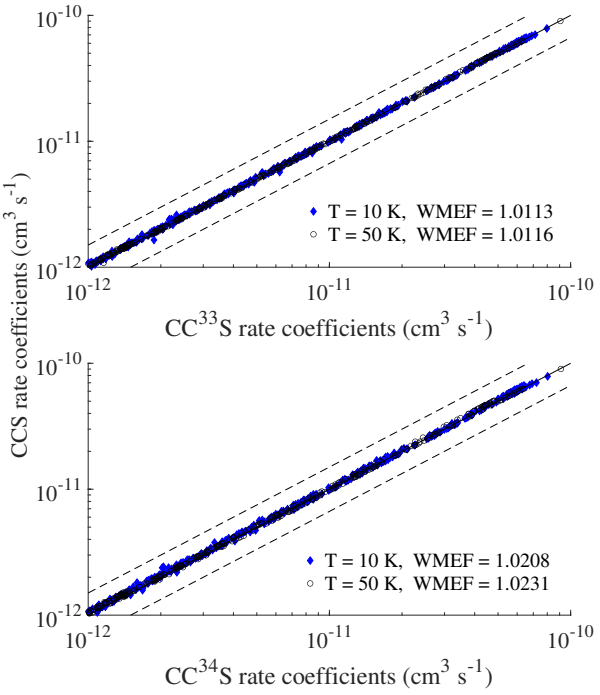

Figure 4. Systematic comparison of de-excitation fine-structure resolved rate coefficients at T = 10 K and 50 K of $^{12}C^{12}C^{33}S$ (upper panel) and $^{12}C^{12}C^{34}S$ (lower panel) isotopologues with respect to the fine rate coefficients of the main isotopologue $^{12}C^{12}C^{32}S$. The plain line represents a perfect agreement, the dashed line represents a deviation of 50%.

$= \Delta j$ over $\Delta F \neq \Delta j$ is greater for $\Delta N = \Delta j$ transitions than for $\Delta N \neq \Delta j$

Propensity rules of $CC^{33}S$ isotopologues are presented in Figure 6. The propensity rules regarding the impact of ΔF on $\Delta N = \Delta j$ (left panel) and $\Delta N \neq \Delta j$ (right panel) rate coefficients are presented.

As for ^{13}CCS and $C^{13}CS$, the dominant transitions in $CC^{33}S$ are $\Delta F = \Delta j$ transitions for both $\Delta N = \Delta j$ and $\Delta N \neq \Delta j$ transitions. The greater the difference between ΔF and Δj is, the more the rate coefficients for the transition decrease. Therefore, rate coefficients with $\Delta F = \Delta j + 1$ are greater than those with $\Delta F = \Delta j + 2$, and similarly, those with $\Delta F = \Delta j + 2$ are greater than those with $\Delta F = \Delta j + 3$ transitions.

To discuss the isotopic effect induced by the position of the ^{13}C on the collisional rate coefficients, hyperfine-structure resolved de-excitation rate coefficients of ^{13}CCS and $C^{13}CS$ isotopologues are systematically compared at 10 K in Figure 7. In the WMEF calculation, ^{13}CCS was considered as the reference, so $k_i^{main} \equiv k_i^{^{13}CCS}$ and $k_i^{sec} \equiv k_i^{C^{13}CS}$.

The similarities between the datasets are quite pronounced with an overall agreement better than 10-15% over the dominant transitions, and better than 40% for any transitions. The WMEF is small and comparable to what have been observed when comparing fine-structure resolved rate coefficients of CCS isotopologues.

3.3 Astrophysical modeling

In this Section, the isotopologues are treated separately according to their structure. First, astrophysical application for fine-structure transitions in CCS and $CC^{34}S$ are considered, and then hyperfine-structure transitions in ^{13}CCS and $C^{13}CS$ are examined. Since the Einstein coefficients for $CC^{33}S$ are not available, no astrophysical applications have been conducted for this isotopologue.

3.3.1 CCS and $CC^{34}S$

The excitation temperature is useful to check the validity of the LTE approximation at a given volume density, i.e. if the population of the energy levels involve in the transition are following a Boltzmann distribution.

In Figure 8, excitation temperatures (higher panels) of three transitions of CCS (black lines) and $CC^{34}S$ (red lines) are plotted against the volume density of the gas at 10 K. The column density for both isotologues have been set at 1×10^{13} cm^{-2} in order to discuss collisional effect. Eventhough this value will be different for all isotologues in practice (probably underestimated for the main isotologue, and overestimated for secondary ones), it is not suppose to influence much the value of T_{ex} as long as the opacity is weak.

Typically, the excitation temperature behaves as follow: at very low volume density, the radiative processes are dominant so $T_{ex} = T_{CMB}$. As the volume density of the medium increases, radiative and collisional processes come into competition, thus characterizing the non-LTE domain where $T_{CMB} < T_{ex} < T_{kin}$. This is typically the domain of densities where inelastic rate coefficients are required to proper model molecular abundances. When collisions dominate, the LTE domain starts, so that $T_{ex} = T_{kin}$, and the population of energy levels are following a Boltzmann distribution, and will only depend on the kinetic temperature of the gas.

The 3_4-2_3 transition follows the general behavior as described above. The 1_2-0_1 transition presents a maser effect (microwave amplification by stimulated emission of radiation) due to a population inversion. This maser covers a large range of volume densities, from 10^3 to 10^6 cm^{-3}, and might be observable in several molecular clouds. The 3_2-2_1 transition presents a so-called sub-thermal effect for volume density ranging from 10^3 to 10^5 cm^{-3}, which means that its excitation temperature is lower than T_{CMB} in this density range. Consequently, this transition might be observable in absorption, contrary to other lines presented here. Such effect is also present at a lower scale in the 1_0-0_1 transition.

None of these lines are thermalized at the typical volume density of molecular clouds (10^4-10^5 cm^{-3}), and reach LTE from volume density of about 10^5-10^6 cm^{-3}. Therefore, accurate determination of CCS and $CC^{34}S$ abundances in molecular clouds would require the use of the fine-structure resolved rate coefficients produced in this work in non-LTE models.

The radiance temperature T_r is of the upmost importance since it can be directly compared to what is measured by telescopes. In the lower panels of Figure 8, the variation of T_r for CCS (black line) and $CC^{34}S$ (red lines) transitions across column densities ranging from between 10^{12} and 10^{15} cm^{-2} is presented at two different volume densities: $n = 10^4$ cm^{-3} (dashed lines) and $n = 10^5$ cm^{-3} (dotted lines).

Radiance temperature for the transitions under discussion here generally increases with the increasing column density of the molecule at both volume densities (as expected for optically thin lines) and reaches a plateau when the lines become optically thick. The exception is the 3_2-2_1 transition, which exhibits a negative ra-

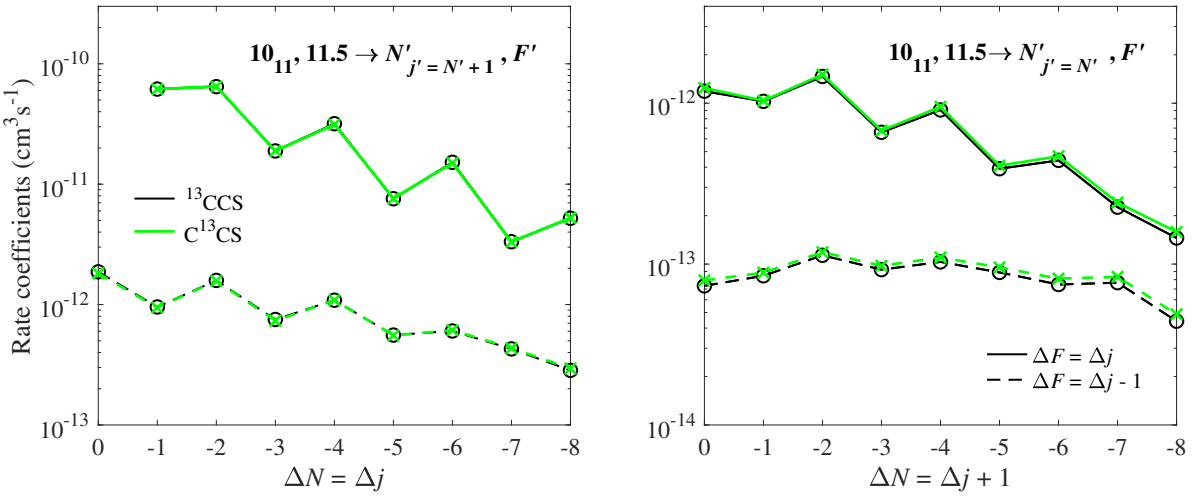

Figure 5. Propensity rules for hyperfine-structure resolved rate coefficients at 10 K for ^{13}CCS (black) and C^{13}CS (green) isotopologues from the 10_{11}, 11.5 level. Rate coefficients for $\Delta F = \Delta j$ (solid lines) and $\Delta F \neq \Delta j$ (dashed lines) are presented for both $\Delta N = \Delta j$ (right panel) and $\Delta N \neq \Delta j$ (left panel) transitions.

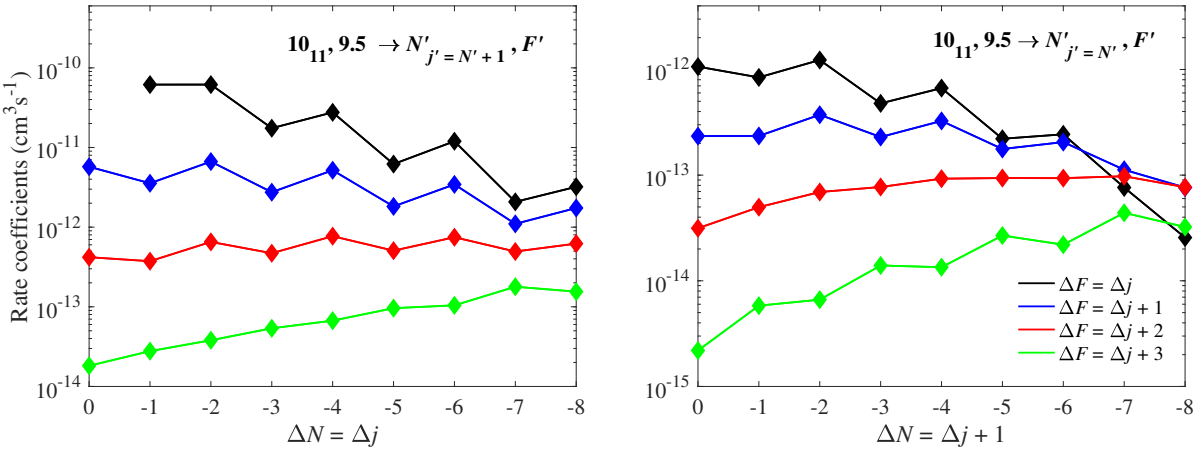

Figure 6. Propensity rules for hyperfine-structure resolved rate coefficients of CC^{33}S isotopologue at 10 K from the 10_{11}, 9.5 level. Rate coefficients for $\Delta F = \Delta j$ (solid lines) and $\Delta F \neq \Delta j$ (dashed lines) are presented for both $\Delta N = \Delta j$ (right panel) and $\Delta N \neq \Delta j$ (left panel) transitions.

diance temperature at a volume density of 10^4 cm^{-3}, characteristic of absorption lines.

The radiance temperature tend to be higher at increased volume density, except for the 1_2-0_1 maser emission when the column density of the molecule is lower than 10^{14} cm^{-2}.

The excitation conditions of the two isotopologues are similar and the effect of isotopic substitution is weak. The excitation temperature for the transitions under consideration here are very similar, eventhough some differences for the 3_2-2_1 transition can be observed within the typical density of molecular clouds. The same remarks hold for the radiance temperature.

3.3.2 ^{13}CCS and $C^{13}CS$

The excitation temperature of two observed lines of ^{13}CCS (black lines) and C^{13}CS (green lines) are presented in the upper panels of Figure 9 against the volume density of the gas at 10 K. Here also, the column density of both isotopologues have been set at 10^{13} cm^{-2}.

The 2_3,3.5 - 1_2,2.5 transition presents a weak suprathermal effect ($T_{ex} > T_{kin}$) for a volume density 10^4-10^5 cm^{-3}. The 1_2,2.5 - 0_1,1.5 transition presents a maser effect for volume density ranging from 10^3 to 10^6 cm^{-3}. Therefore, the use of the rate coefficients provided in this work is recommended for a reliable determination of ^{13}CCS and C^{13}CS abundances in molecular clouds.

The excitation temperatures of both isotopologues have the same behavior and very similar values, eventhough some slight descrepencies can be observed. The excitation temperatures of the

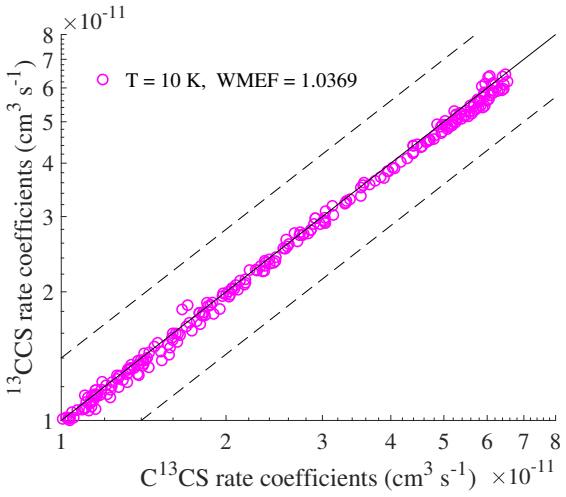

Figure 7. Systematic comparison of dominant de-excitation hyperfine-structure resolved rate coefficients at T = 10 K of the $^{13}C^{12}C^{32}S$ (x-axis) and $^{12}C^{13}C^{32}S$ (y-axis) isotopologues. The plain line represents a perfect agreement between the two data sets and the dashed line a deviation of 50%.

$C^{13}CS$ are slightly shifted towards higher volume densities compared to the excitation temperatures of ^{13}CCS.

The radiance temperatures for transitions of ^{13}CCS (black lines) and $C^{13}CS$ (green lines) as a function of their column density ranging from 10^{10} and 10^{14} cm^{-2} is represented in the lower panels of Figure 9 at two volume densities of the gas: $n = 10^4$ cm^{-3} (dashed lines) and $n = 10^5$ cm^{-3} (dotted lines).

The radiance temperatures are generally higher at lower gas densities (dashed lines), likely due to suprathermal and maser effects.

In the work of Sakai et al. (2007), $C^{13}CS$ abundance has been found to be 4.2 times larger than that of ^{13}CCS based on LTE modeling. The production mechanism of CCS was assumed to be the cause of such differences between $C^{13}CS$ and ^{13}CCS isotopologues. Another possible explanation would have been to consider that the levels of $C^{13}CS$ involved in the observed transitions were more efficiently populated by collisions. However, the weak effect for the isotopic substitution in the collisional data observed between the two ^{13}C-bearing isotopologues is not strong enough to explain such anomaly. Thus, the formation and destruction paths of the isotopologues are probably the source of the discrepancies in ^{13}CCS and $C^{13}CS$ abundances.

4 CONCLUSIONS

In this work, the very first state-to-state rate coefficients were provided for detectable CCS isotopologues: ^{13}CCS, $C^{13}CS$, $CC^{34}S$ and $CC^{33}S$. Scattering calculations were perfomed with the Close-Coupling approach for all four isotopologues in collision with He explicitely accounting for their fine structure, to derive rate coefficients for the 5-50 K temperature range. The hyperfine structures induced by the nuclear spin of ^{13}C ($I = \frac{1}{2}$) and ^{33}C ($I = \frac{3}{2}$) were considered to provided hyperfine-structure resolved rate coefficients using the recoupling approach for the 5-15 K temperature range for ^{13}CCS, $C^{13}CS$ and $CC^{33}S$ isotopologues.

The sets of rate coefficients of CCS, ^{13}CCS, $C^{13}CS$ and $CC^{34}S$ isotopologues have been used in radiative transfer analysis, and all commonly observed transitions have been found to have a population not following a Boltzmann distribution at typical volume density of molecular clouds (10^4-10^5 cm^{-3}), showing that the data provided in this work must be used to properly model CCS isotopologues observations in molecular clouds.

For such models, rate coefficients for CCS isotopologues in collision with $H_2(j = 0)$ are required. Here, they have been infered by scaling the rate coefficients of CCS isotopologues in collision with He computed in this work. Performing calculations for the CCS-H_2 ($j = 0$), however difficult regarding the complexity of the internal structure of CCS isotopologues, would be interesting to confirm the results obtained here.

The effect of the isotopic subsititution on the fine and hyperfine structure rate coefficients have been studied and was found to be weak for all isotopic substitutions but stronger for ^{13}CCS and $CC^{34}S$,which exhibit larger shifts of the c.o.m. in the PES representation. The differences between hyperfine-structure rate coefficients of ^{13}CCS and $C^{13}CS$ isotopologue appear to be stronger than on the fine-structure resolved rate coefficients only.

The effect of the deviation in the sets of rate coefficients on the excitation and radiance temperature have been found to be weak for all transitions. Therefore, according to the precision requested to interpret observations, the fine-structure resolved rate coefficients of CCS could be use to model $CC^{34}S$; the hyperfine-structure resolved rate coefficients of ^{13}CCS could be use to model $C^{13}CS$, and vice-versa. Therefore, It is then possible to limit the number of isotopologues under consideration if one wants to extend the temperature range of CCS isotopologues collisional data.

The anomaly between ^{13}CCS and $C^{13}CS$ abundances reported in the work of Sakai et al. (2007) cannot be explained by collisional excitation effects, and need to be further discussed based on reliable abundances of the two ^{13}C-based isotopologues derived by using the hyperfine-structure rate coefficients provided in this work.

ACKNOWLEDGEMENTS

We acknowledge Professor Cernicharo for initiating this project and for fruitful discussions.

We acknowledge financial support from the European Research Council (Consolidator Grant COLLEXISM, Grant Agreement No. 811363). We wish to acknowledge the support from the CEA/GENCI (Grand Equipement National de Calcul Intensif) for awarding us access to the TGCC (Très Grand Centre de Calcul) Joliot Curie/IRENE supercomputer within the A0110413001 project. We also acknowledge Rennes Metropole for financial support. F.L. acknowledges the Institut Universitaire de France.

DATA AVAILABILITY

The computed collisional data for the 5 CCS isotopologues studied here (CCS, ^{13}CCS, $C^{13}CS$, $CC^{33}S$ and $CC^{34}S$) in collision with He will be available on the following databases: BASECOL (Dubernet et al. 2012), LAMDA (Van der Tak et al. 2020) and EMAA (Faure et al. 2021).

REFERENCES

Alexander M. H., Dagdigian P. J., 1983, J. Chem. Phys., 79, 302
Alexander M. H., Dagdigian P. J., 1985, The Journal of Chemical Physics, 83, 2191

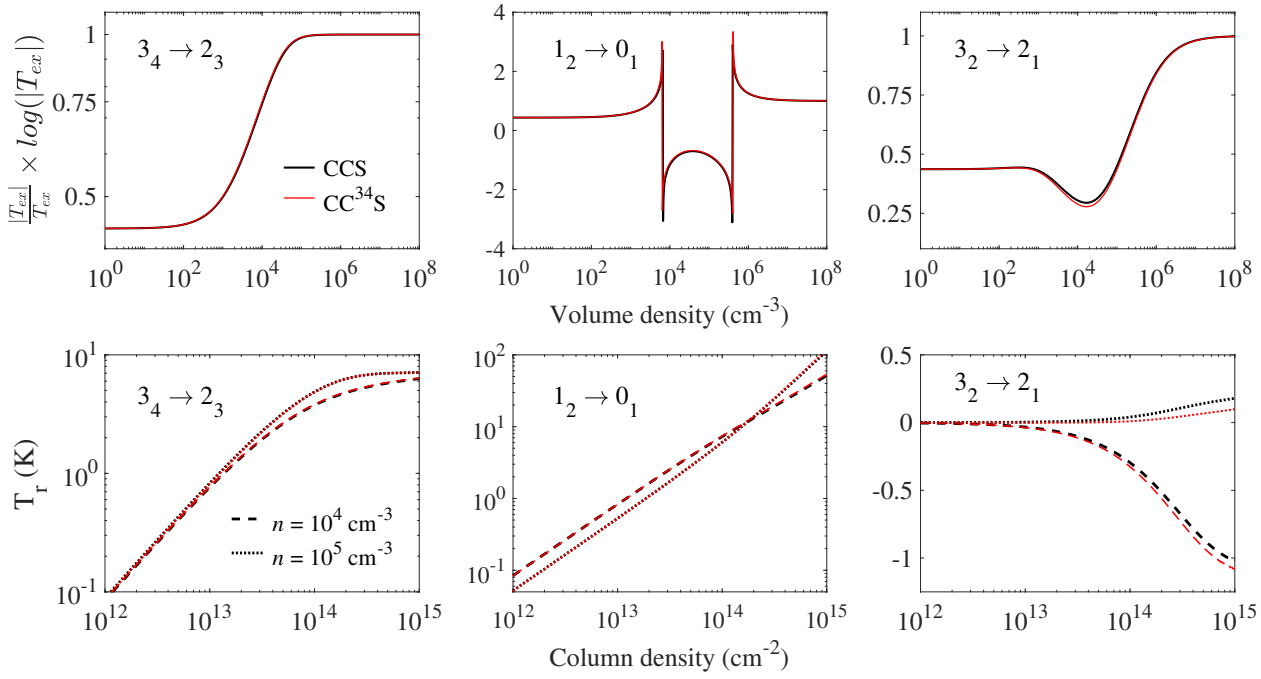

Figure 8. In the upper panels, excitation temperatures of two observed transitions of CCS (black lines) and CC^{34}S (red lines) against the volume density of the gas. In the lower panels, radiance temperature for the same transitions as a function of the column density of the isotopologues at two volume densities of the gas: $n = 10^4$ cm^{-3} (dashed lines) and $n = 10^5$ cm^{-3} (dotted lines). The kinetic temperature of the gas was set at 10 K.

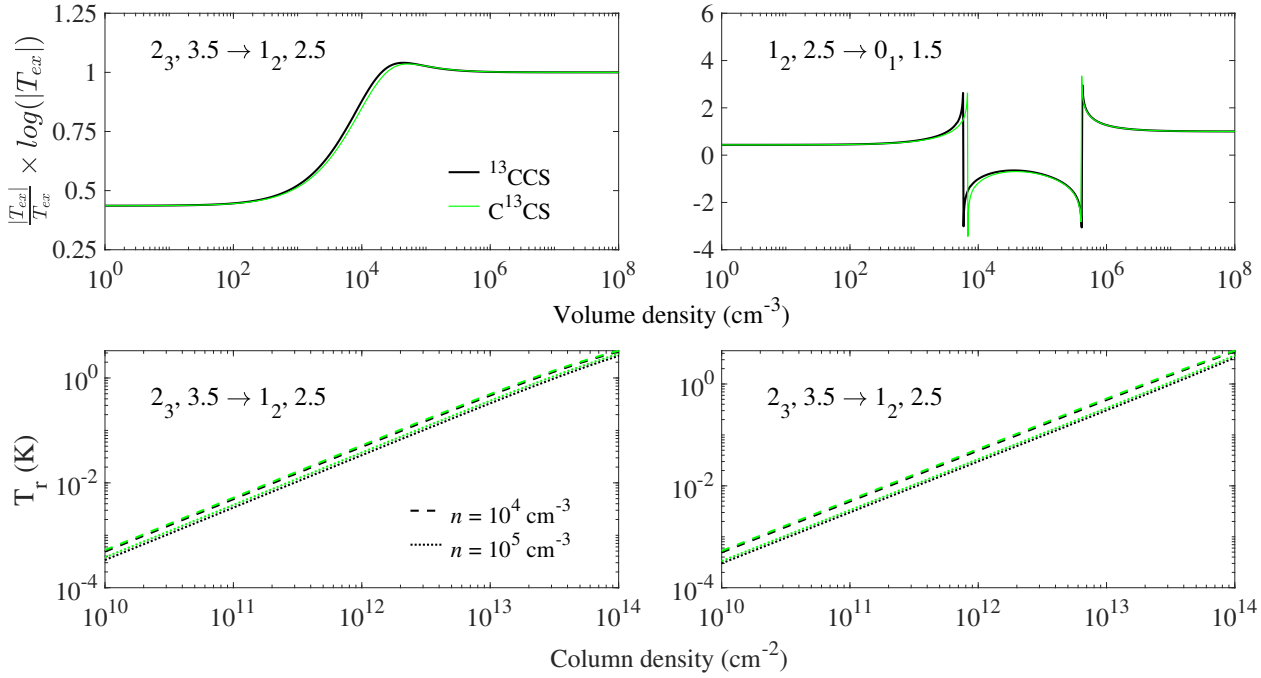

Figure 9. In the upper panels, excitation temperatures of two observed transitions of ^{13}CCS (black lines) and C^{13}CS (green lines) against the volume density of the gas. In the lower panels, radiance temperature for the same transitions as a function of the column density of the isotopologues at two volume densities of the gas: $n = 10^4$ cm^{-3} (dashed lines) and $n = 10^5$ cm^{-3} (dotted lines). The kinetic temperature of the gas was set at 10 K.

Boys S., Bernardi F., 1970, Mol. Phys., 19, 553
Buffa G., 2012, Monthly Notices of the Royal Astronomical Society, pp no–no
Costes M., Naulin C., 2016, Chem. Sci. J., 7, 2462
Cybulski S. M., Toczyłowski R. R., 1999, J. Chem. Phys., 111, 10520
Dagdigian P. J., 2018, Monthly Notices of the Royal Astronomical Society, 479, 3227
Dagdigian P. J., 2022, Monthly Notices of the Royal Astronomical Society, 514, 2214
Daniel F., Dubernet M.-L., Meuwly M., 2004, The Journal of Chemical Physics, 121, 4540
Deegan M. J., Knowles P. J., 1994, Chem. Phys. Lett., 227, 321
Dixon R. N., Field D., 1979, Proceedings of the Royal Society of London. A. Mathematical and Physical Sciences, 366, 225
Dumouchel F., Kłos J., Toboła R., Bacmann A., Maret S., Hily-Blant P., Faure A., Lique F., 2012, J. Chem. Phys., 137, 114306
Dumouchel F., Lique F., Spielfiedel A., Feautrier N., 2017, Monthly Notices of the Royal Astronomical Society, 471, 1849
Endres C. P., Schlemmer S., Schilke P., Stutzki J., Müller H. S., 2016, Journal of Molecular Spectroscopy, 327, 95
Faure A., Lique F., 2012, Monthly Notices of the Royal Astronomical Society, 425, 740
Flower D. R., Lique F., 2015, Monthly Notices of the Royal Astronomical Society, 446, 1750
Fuente A., Cernicharo J., Barcia A., Gómes-Gonzáles 1990, Astron. Astrophys., 231, 151
Fuentetaja R., et al., 2023, in prep.
Godard Palluet A., Lique F., 2023, The Journal of Chemical Physics, 158, 044303
Hily-Blant P., Faure A., Vastel C., Magalhaes V., Lefloch B., Bachiller R., 2018, Monthly Notices of the Royal Astronomical Society, 480, 1174
Hutson J., Green S., 1994, Molscat Computer Program, Version 14, Distributed by Collaborative Computational Projet No. 6 of the UK Science and Engineering Research Council
Ikeda M., Sekimoto Y., Yamamoto S., 1997, Journal of Molecular Spectroscopy, 185, 21
Kalugina Y., Lique F., Kłos J., 2012, Monthly Notices of the Royal Astronomical Society, 422, 812
Lique F., Bulut N., Roncero O., 2016, Monthly Notices of the Royal Astronomical Society, 461, 4477
Loison J.-C., Wakelam V., Gratier P., Hickson K. M., 2020, Monthly Notices of the Royal Astronomical Society, 498, 4663
Manolopoulos D. E., 1986, J. Chem. Phys., 85, 6425
McGuire B. A., 2022, The Astrophysical Journal Supplement Series, 259, 30
McGuire B. A., Martin-Drumel M.-A., Lee K. L. K., Stanton J. F., Gottlieb C. A., McCarthy M. C., 2018, Phys. Chem. Phys. Chem., 20, 13870
Müller H. S. P., Thorwirth S., Roth D. A., Winnewisser G., 2001, Astronomy & Astrophysics, 370, L49
Müller H. S., Schlöder F., Stutzki J., Winnewisser G., 2005, Journal of Molecular Structure, 742, 215
Navarro-Almaida D., et al., 2023, Astronomy & Astrophysics, 670, A110
Ndaw D., Bop C. T., Dieye G., Faye N. A. B., Lique F., 2021, Monthly Notices of the Royal Astronomical Society, 503, 5976
Pickett H. M., Poynter R. L., Cohen E. A., Delitsky M. L., Pearson J. C., Muller H. S. P., 1998, J. Quant. Spectrosc. Radiat. Transfer, 60, 883
Pirlot Jankowiak P., Lique F., Dagdigian P. J., 2023a, Monthly Notices of the Royal Astronomical Society, 523, 3732
Pirlot Jankowiak P., Lique F., Dagdigian P. J., 2023b, Monthly Notices of the Royal Astronomical Society, 526, 885
Sakai N., Ikeda M., Morita M., Sakai T., Takano S., Osamura Y., Yamamoto S., 2007, Astrophys. J., 663, 1174
Suzuki H., Yamamoto S., Ohishi M., Kaifu N., Ishikawa S.-I., Hirahara Y., Takano S., 1992, Astron. Astrophys., 392, 551
Takano S., et al., 1998, Astron. Astrophys., 329, 1156
Taniguchi K., Ozeki H., Saito M., Sakai N., Nakamura F., Kameno S., Takano S., Yamamoto S., 2016, The Astrophysical Journal, 817, 147
Velusamy T., Kuiper T. B. H., Langer W. D., 1995, Astrophys. J., 451, L75
Wernli M., Wiesenfeld L., Faure A., Valiron P., 2007, Astronomy & Astrophysics, 464, 1147
Wolkovitch D., Langer W. D., Goldsmith P. F., Heyer M., 1997, Astrophys. J., 477, 241
van der Tak F. F. S., Black J. H., Schöier F. L., Jansen D. J., van Dishoeck E. F., 2007, Astronomy & Astrophysics, 468, 627

APPENDIX A: FINE STRUCTURE ENERGY LEVELS OF CCS ISOTOPOLOGUES

This paper has been typeset from a TEX/LATEX file prepared by the author.

Table A1. List of fine structure energy levels of the CCS, ^{13}CCS, C^{13}CS, CC^{34}S and CC^{33}S istopologues based on the spectroscopic constants from McGuire et al. (2018) and Fuentetaja et al. (2023).

Label N_j	Energy (cm^{-1})				
	CCS	^{13}CCS	C^{13}CS	CC^{34}S	CC^{33}S
1_0	0.00000	0.00000	0.00000	0.00000	0.00000
0_1	0.37091	0.35707	0.36947	0.36416	0.36744
1_2	1.11623	1.07412	1.11184	1.09568	1.10568
2_3	2.24205	2.15627	2.23311	2.20018	2.22054
3_4	3.75574	3.6098	3.74048	3.68447	3.71909
4_5	5.66470	5.4412	5.64129	5.55549	5.60851
1_1	6.48371	6.48428	6.48578	6.48368	6.48537
2_1	6.54495	6.54004	6.54641	6.54220	6.5451
2_2	7.34800	7.30993	7.34597	7.32905	7.33989
3_2	7.52821	7.474279	7.52441	7.50141	7.51599
5_6	7.97567	7.65654	7.94217	7.81964	7.89535
3_3	8.64444	8.54840	8.63625	8.59709	8.62167
4_3	8.99525	8.86905	8.98370	8.93300	8.96467
4_4	10.3730	10.1997	10.3566	10.2878	10.3307
6_7	10.6944	10.2610	10.6488	10.4824	10.5852
5_4	10.9387	10.7181	10.9171	10.8302	10.8841
5_5	12.5337	12.2638	12.5071	12.4012	12.4670
6_5	13.3512	13.0148	13.3172	13.1859	13.2673
7_8	13.8256	13.2589	13.7659	13.5483	13.6827
6_6	15.1266	14.7407	15.0876	14.9373	15.0305
7_6	16.2259	15.7533	16.1773	15.9939	16.1075
8_9	17.3730	16.6538	17.2971	17.0210	17.1916
7_7	18.1515	17.6304	18.0982	17.8960	18.0212
8_7	19.5570	18.9282	19.4918	19.2485	19.3991
9_{10}	21.3395	20.4486	21.2455	20.9035	21.1147
8_8	21.6086	20.9329	21.5388	21.2773	21.4392
9_8	23.3400	22.5353	23.2561	22.9453	23.1375
9_9	25.4978	24.6481	25.4095	25.0813	25.2843
10_{11}	25.7276	24.6456	25.6133	25.1980	25.4545
10_9	27.5709	26.5709	27.4662	27.0806	27.3190
10_{10}	29.8190	28.7761	29.7103	29.3079	29.5567
11_{12}	30.5391	29.2465	30.4025	29.9063	30.2127
11_{10}	32.2468	31.0322	32.1193	31.6513	31.9405
11_{11}	34.5723	33.3169	34.4410	33.9572	34.2563
12_{13}	35.7755	34.2529	35.6145	35.0300	35.3909
12_{11}	37.3654	35.9167	37.2130	36.6553	36.9999
12_{12}	39.7577	38.2705	39.6018	39.0290	39.3830
13_{14}	41.4378	39.6658	41.2504	40.5702	40.9902
13_{12}	42.9246	41.2228	42.7453	42.0906	42.4951
13_{13}	45.3751	43.6367	45.1925	44.5234	44.9369
14_{15}	47.5272	45.4863	47.3112	46.5279	47.0115
14_{13}	48.9231	46.9490	48.7148	47.9557	48.4246
14_{14}	51.4246	49.4156	51.2132	50.4404	50.9179
15_{16}	54.0442	51.7150	53.7976	52.9037	53.4555
15_{14}	55.3596	53.0939	55.1203	54.2494	54.7873
15_{15}	57.9060	55.6073	57.6639	56.7799	57.3259
16_{17}	60.9895	58.3527	60.7103	59.6983	60.3230
16_{15}	62.2331	59.6567	61.9608	60.9708	61.5823
16_{16}	64.8194	62.2116	64.5445	63.5419	64.1612
17_{18}	68.3637	65.3997	68.0497	66.9122	67.6144
17_{16}	69.5429	66.6366	69.2356	68.1190	68.8086
17_{17}	72.1648	69.2286	71.8550	70.7265	71.4235
18_{19}	76.1670	72.8565	75.8162	74.5459	75.3300
18_{17}	77.2883	74.0329	76.9439	75.6935	76.4657
18_{18}	79.9421	76.6582	79.5954	78.3335	79.1128
19_{20}	84.3998	80.7235	84.0103	82.5995	83.4703
19_{18}	85.4688	81.8451	85.0852	83.6936	84.5529
19_{19}	88.1513	84.5004	87.7656	86.3630	87.2292
20_{21}	93.0626	89.0009	92.6321	91.0735	92.0355
20_{19}	94.0839	90.0727	93.6592	92.1189	93.0700
20_{20}	96.7924	92.7552	96.3658	94.8149	95.7725